Title
Opportunistic Breast Density Assessment in Women Receiving Low-dose Chest Computed Tomography Screening

Journal
Academic Radiology, 23(9)

ISSN
1076-6332

Authors
Chen, Jeon-Hor
Chan, Siwa
Lu, Nan-Han
et al.

Publication Date
2016-09-01

DOI
10.1016/j.acra.2016.05.003

Peer reviewed

HHS Public Access

Author manuscript

Acad Radiol. Author manuscript; available in PMC 2017 September 01.

Published in final edited form as:

Acad Radiol. 2016 September ; 23(9): 1154–1161. doi:10.1016/j.acra.2016.05.003.

Opportunistic Breast Density Assessment in Women Receiving Low Dose Chest Computed Tomography Screening

Jeon-Hor Chen[1,2,*], **Siwa Chan**[3,4], **Nan-Han Lu**[2], **Yifan Li**[1], **Yu Chieh Tsai**[5], **Po Yun Huang**[5], **Chia-Ju Chang**[5], and **Min-Ying Su**[1]

[1]Center for Functional Onco-Imaging, Department of Radiological Sciences, University of California, Irvine, CA, United States

[2]Department of Radiology, E-Da Hospital and I-Shou University, Kaohsiung, Taiwan

[3]Department of Radiology, Taichung Veterans General Hospital, Taichung, Taiwan

[4]Graduate Institute of Biomedical Electronics and Bioinformatics, National Taiwan University, Taipei, Taiwan

[5]Department of Radiological Technology, China Medical University, Taichung, Taiwan

Abstract

Rationale and Objectives—Low dose chest computed tomography (LDCT), increasingly being used for screening of lung cancer, may also be used to measure breast density, which is proven as a risk factor for breast cancer. In this study we developed a segmentation method to measure quantitative breast density on CT images and correlated with MR density.

Materials and Methods—Forty healthy females receiving both LDCT and breast magnetic resonance imaging (MRI) were studied. A semi-automatic method was applied to quantify the breast density on LDCT images. The intra-, inter-operator reproducibility was evaluated. The volumetric density on MRI was obtained by using a well-established automatic template-based segmentation method. The breast volume (BV), fibroglandular tissue volume (FV), and percent breast density (PD) measured on LDCT and MRI were compared.

Results—The measurements of BV, FV, and PD on LDCT images yields highly consistent results, with the intraclass correlation coefficient (ICC) of 0.999 for BV, 0.977 for FV, and 0.966 for PD for intra-operator reproducibility; and ICC of 0.953 for BV, 0.974 for FV, and 0.973 for PD for inter-operator reproducibility. The BV, FV, and PD measured on LDCT and MRI were well correlated (all $r \geq 0.90$). Bland-Altman plots showed that a larger BV and FV were measured on LDCT compared with MRI.

Conclusions—The preliminary results showed that quantitative breast density can be measured from LDCT, and that our segmentation method could yield a high reproducibility on the measured

[*]Corresponding Author: **Jeon-Hor Chen, M.D.**, John Tu and Thomas Yuen Center for Functional Onco-Imaging, 164 Irvine Hall, University of California, Irvine, CA 92697-5020, USA, Tel: (949) 824-9327, Fax: (949) 824-3481, jeonhc@uci.edu.

volume and percent breast density. The results measured on LDCT and MRI were highly correlated. Our results showed that LDCT may provide valuable information about breast density for evaluating breast cancer risk.

Introduction

Mammographic density (MD) has been proven as an independent risk factor for breast cancer (1-2). Women with dense breast tissue visible on a mammogram have a cancer risk 1.8 to 6.0 times that of women with little density (3). A great research effort has been devoted to incorporate breast density into risk prediction models to better estimate each individual's cancer risk. Because the 2D mammography-based measurement is subject to tissue overlapping thus not able to provide true volumetric information, other emerging technologies based on 3-dimensional imaging for assessing breast density are being developed. Among these new modalities, MRI is most well studied (4-6). Although breast MRI is suitable for volumetric analysis and segmentation tools are available, not many women can receive breast MRI due to its high cost. Currently, only high risk women with lifetime breast cancer risks more than twenty percent will receive breast MRI for screening (7).

Low dose chest computed tomography (LDCT) is increasingly being used for the screening of lung cancer (8-10) and diagnosis of other pulmonary diseases (11, 12). According to a report from The National Lung Screening Trial (NLST), there was a 20 percent reduction in deaths from lung cancer among current or former heavy smokers who were screened with LDCT compared with those screened by chest X-ray (9). The overall average effective dose was approximately 2 mSv for LDCT, which was much lower compared with an average effective dose of 7 mSv for a typical standard-dose chest CT examination (13). Despite of general radiation concern, LDCT is considered a safe screening tool, and its clinical use is anticipated to increase. Among the examinees, more than 40% are female (9). As its popularity in clinical practice increases, besides lung cancer screening, LDCT has potential to provide additional information about breast density for personalized management of breast cancer screening.

Quantification of breast density using LDCT is, however, challenging due to the noisy imaging quality (14, 15), which makes the segmentation of the fibroglandular tissue difficult. Robust segmentation algorithms thus are required. A quantitative density segmentation method for LDCT was reported recently, showing that breast density measured from LDCT was lower than mammographic density (22±0.6 % vs. 34±1.9 %), but with a high Pearson correlation coefficient of r=0.88 (16).

Our group has developed an automatic 3D MR-based method for breast density segmentation using sophisticated computer-assisted algorithms (17). In this study we modified the method for segmentation on LDCT to explore the potential role of LDCT as a new density measurement method. We evaluated the intra- and inter-operator reproducibility; and further, compared the volumetric density results analyzed from LDCT with those analyzed from 3D MRI as the ground truth.

Materials and Methods

Subjects

This study was approved by the institutional review board and complied with the Health Insurance Portability and Accountability Act. From Feb. 2009 to Oct. 2011, 40 healthy Asian female subjects (mean age 57, range 34-81) who had both LDCT and breast MRI performed within one year of each other were studied. The imaging was done as part of the physical examination package. These women chose to receive LDCT for detection of early lung lesions and breast MRI for detection of early breast cancer. Dynamic contrast enhanced (DCE) breast MRI was done. No breast lesion was found in any subject, thus results from bilateral breasts were included in the analysis.

Imaging Studies

Low Dose Chest CT—The non-contrast-enhanced LDCT images were acquired with the examined women in supine position using a GE multi-detector CT scanner (GE LightSpeed VCT). The imaging parameters were: Kvp=120, X-ray tube current=50mA, slice thickness=5mm, field of view=340mm, matrix= 512×512, and voxel size= 0.66×0.66×5 mm^3. In this study only the CT images covering the breast region were used for the breast density analysis.

Breast MR Imaging—The breast MR images were acquired with the examined women in prone position at a 1.5T GE MR scanner (GE SIGNA HDx). An eight-channel breast coil was used. Non-contrast-enhanced axial fast spin echo T1W images were acquired first, followed by DCE-MRI. In this study, only the non-enhanced T1W images were used for the density analysis. The imaging parameters for the T1WI were: acquisition type=2D, repetition time=583msce, echo time=8.6msec, flip angle=90 degrees, slice thickness=5mm, spacing between slices=5mm, number of average=0.5, percent sampling=57%, echo train length=3, field of view=280×280mm, matrix=512×512, and voxel size=0.55×0.55×5.00 mm^3.

Breast Segmentation and Quantification of Breast Density

Since the LDCT density segmentation method was newly developed, we first conducted intra- and inter-operator consistency studies (performed by TYC and PYH) based on 10 randomly selected subjects from the cohort. After this initial reproducibility analysis, one operator (TYC) who had a better reproducibility was chosen to perform the segmentation on LDCT and breast MR images of the remaining 30 subjects.

Breast Density Analyzed from LDCT—For LDCT-based breast segmentation, there were two major challenges. Firstly, the chest wall cannot be easily removed by intensity-based methods because of its similar brightness level with that of fibroglandular tissue on the images. Secondly, the images are noisy, which makes segmentation of fibroglandular tissue more difficult. The segmentation methodology has three procedures: the image preprocessing, breast segmentation and fibroglandular tissue segmentation.

The image intensities within the entire CT imaging slab were in a range around 30,000, and it had a low contrast in the breast region. Therefore, the first step was to rescale the gray level in order to enhance the contrast. The gray level histogram of LDCT has two peaks. The first peak includes dark signal coming from background, lung and fat tissue; and the second peak contains the fibroglandular tissue, bones, and muscles. The histogram was fitted to separate the two peaks, and the beginning point of the second peak was used as a threshold to remove tissues contained within the first peak.

To define the posterior boundary of the breast, a horizontal line that connects the lateral margin of the pectoralis muscles at the aortic arch level was manually drawn, and this line was applied to all slices as an anatomic landmark to remove the posterior non-breast tissues (**Figure 1**). The operator could adjust the line dorsally to ensure that all the fibroglandular tissue was included. The superior and inferior boundaries of the breast were defined by comparing the thickness of breast fat with the body fat. The subcutaneous fatty tissue of the non-breast (body) region on the chest typically displays homogeneous thickness across the chest wall, which could be used to determine where the breast starts and ends.

Further, the tissues inside the thoracic cavity region needed to be removed using morphological processing, as shown in **Figure 2**. The dark region of the left and right lungs were first identified as a mark (**Figure 2b**), and then this mask was expanded using morphological dilation to cover all bright regions (heart and aorta) between the two lungs to define the thoracic cavity region on the imaging slice (**Figure 2c**). After removing the thoracic cavity region, the bilateral breast regions, including the chest wall, can be obtained (**Figure 2d**). The obtained breast region on this slice was then used as the template for the adjacent superior and inferior slices, following the procedure developed for segmenting breast region on MRI (16), and the process continued until reaching the beginning and ending slices. On a case-by-case basis, the operator may need to do some fine adjustments to cover the entire breast without cutting out any fibroglandular tissue. To further remove the chest wall, we used several morphological methods and fuzzy-C-means (FCM) segmentation algorithm to obtain the edge of the chest wall region, following the methods developed for removing chest wall muscle on MRI (detailed procedures were described in (16)).

For the segmentation of fibroglandular tissue, a Gaussian median filter was incorporated into the processing to reduce the effects of random noise. The contrast of the image was also enhanced to make the fibroglandular tissue brighter. A FCM algorithm with a cluster number of 9 or 10 was used, and 2 or 3 of them were selected to define the fibroglandular tissue. For each case, the segmented breast and fibroglandular tissues were inspected by a radiologist to confirm that they were done correctly. If further modification was needed, the operator might run the analysis program again with different settings, or perform manual corrections.

Breast Density Acquired from MRI—The MR density measurement was based on our well-established template-based automatic segmentation method (17). With the method, the chest body region on a middle slice of the acquired 3D imaging slab was used as the template. Within the chest template, three body landmarks (thoracic spine and bilateral boundary of the pectoral muscle) were identified for performing the initial V-shape cut to determine the posterior lateral boundary of the breast. The chest template was mapped to

each subject's image space to obtain a subject-specific chest model for exclusion. The chest and muscle boundaries determined on the middle slice were used as the reference for the segmentation of adjacent slices, and the process continued superiorly and inferiorly until all 3D slices were segmented.

After the segmentation of the whole breast region was completed, the fuzzy-C-means (FCM) clustering method was used to segment the fibroglandular tissue (5). A bias-field correction algorithm combining nonparametric nonuniformity normalization (N3) and FCM was applied to correct for the signal intensity inhomogeneity (18), and a total cluster number of ($k = 6$) was used to separate the fibroglandular tissue (the lower three intensity clusters) and the fatty tissue (the higher three intensity clusters).

Statistics

Statistical analyses were performed using statistical package SPSS for Windows (V.20.0, IBM, Chicago, Illinois, USA). The consistency tests for LDCT segmentation, including intra- and inter-operator measurements of BV, FV, and PD were evaluated by calculating the intraclass correlation coefficient (ICC) based on a two-way ANOVA with random effects, assuming each series of measurements was done ‘independently’. The analysis was performed using per breast basis, and results from the left and the right breast in each subject were treated as separate variables. For correlation between LDCT and MRI, the analysis was performed using per subject basis, based on averaged results from the left and right of each subject. The results of breast volume (BV), fibroglandular tissue volume (FV), and percent breast density (PD) measured on LDCT and MRI were compared using the Pearson correlation and the Bland-Altman plot.

Results

Assessment of Measurement Reproducibility Using LDCT

The analysis was done using 20 breasts of 10 randomly selected subjects. The reproducibility between two sets of measurements done by the same operator (TYC) was highly consistent, with ICC =0.999 for BV, ICC=0.977 for FV, and ICC=0.966 for PD, respectively. The consistency between two sets of measurements done by two different operators was also very high, with ICC=0.953 for BV, ICC=0.974 for FV, and ICC=0.973 for PD, respectively.

Correlation of Breast Density Measured on LDCT and MRI

Table 1 summarized the measured BV, FV, and PD from LDCT and MRI. **Figure 3** shows the correlation between LDCT- and MR-based measurements of BV, FV, and PD. The Pearson correlation coefficients were r=0.91 for BV, r=0.94 for FV, and r=0.90 for PD, respectively. The unity line was also plotted as the reference, which shows that most analyzed cases have a higher BV and FV measured by LDCT than MRI. **Figure 4** showsthree Bland-Altman plots using MRI-measured results as the gold standard reference. The y-axis shows the difference as (LDCT- MR) measurement. As noted, LDCT tended to have larger BV and FV results compared with the measurements obtained using MRI, showing a positive difference greater than zero. There were two outliers in the BV

comparison, and three outliers in the FV comparison. **Figures 5-7** showed three case examples of LDCT- and MR-based breast density segmentation. **Figure 5** is a pre-menopausal woman. **Figures 6 and 7** are post-menopausal women. **Table 2** showed the results of density measurements in the three subjects. As noted, the BV, FV, and PD acquired from LDCT were all larger than those measured from MRI in these three subjects. The resulted PD as a ratio of FV/BV was, however, very similar.

Discussion

The clinical significance of breast density has attracted a high public attention in recent years. Starting from 2009, nineteen states have passed mandatory breast density reporting laws. Another 13 states are either working on breast density reporting laws or have already introduced legislation. At the national level, The Breast Density and Mammography Reporting Act (H.R.1302) was introduced in the U.S. Congress in October 2011, which requires every mammography report to provide information regarding the patient's breast density (19). Currently the BIRADS score of I to IV based on radiologists' subjective assessment is being reported, which is a coarse qualitative measure. As the H. R. 1302 Breast Density Act is being proactively debated, quantitative imaging methods are also being developed to provide a robust, reproducible and accurate clinical measurement of breast density (20). Many research studies are investigating how the breast density can be used in disease management, e.g. incorporating density into risk assessment model for risk-based screening; or using the change of density after hormonal therapy to predict which patients will benefit from the treatment. A reliable quantitative measurement of breast density is required before these potential clinical applications can be implemented.

Because of limitations of mammography-based measurement in quantification of breast density and the relatively high cost of MRI, other emerging new technologies are being developed for assessing density, including x-ray-based imaging modalities (21, 22), optical imaging modalities (23, 24), and ultrasound-based imaging (25, 26). Efforts have been made to measure breast density from clinical standard chest CT study (27), LDCT (28, 29), cone beam CT (30), and dedicated breast CT (31, 32). Among these, LDCT is used as a clinical exam for lung cancer screening and the number of performed LDCT is increasingly rapidly. With the full coverage of whole chest area and the soft tissue contrast presented on LDCT, the images can be exploited for analysis of breast density in the female subjects.

Breast density on CT can be assessed qualitatively similar to BIRADS categorization (27), or quantitatively (28-32). For quantitative measurement, since breast fatty tissue is continuous with the body fat, the anatomic landmark used for the segmentation of breast boundary will affect the calculation of breast volume, and hence percent breast density (29). To define the breast boundary, in this study, we drew a horizontal line connecting the lateral margin of the bilateral pectoralis muscle at the aortic arch level. If needed, the line could be moved posteriorly, to ensure that all fibroglandular tissue in the bilateral breasts in the entire imaging slab was included.

Since the original images of LDCT were very noisy, in order to facilitate a precise segmentation of fibroglandular tissue, an efficient denoise algorithm was needed to improve

the imaging quality. In this study, we used a Gaussian median filter to remove the random noise. The denoising procedures for LDCT, including filtering algorithms and reconstruction techniques, have been proposed (33). Filtration can be performed in the spatial domain or in the transformed domain. In the spatial domain, the Gaussian is one of the filters which are most frequently used based in the local region (33). With the algorithm, the boundary between the fatty tissue and the fibroglandular tissue became visually distinguishable, which could facilitate the segmentation of the fibroglandular tissue. However, this algorithm would lead to more blurred images, thus more effective methods, such as bilateral filter (34) and neighborhood filter (35) have been proposed.

Although our LDCT density method could achieve decent segmentation quality and a satisfactory reproducibility, in some cases the measurement variation could be high. With the standardized method and criteria for the breast and the fibroglandular tissue segmentation, one major source of variation was from the manual drawing of the posterior breast boundary. Therefore, the training of the operator to reach a high level of consistency based on each individual subject's anatomy to draw this line is very important. The operator who performed all analysis had an extremely high intra-operator ICC of 0.99 for BV measurements.

Our results showed that the measured BV, FV, and PD from LDCT and MRI were highly correlated. Using Bland-Altman to analyze the measurement difference, it was noted that BV measured on LDCT was higher than the BV measured on MRI. Obviously one possible explanation could be due to the different body positions. LDCT was acquired with the subject in supine position and the breast tissues were dragged down by gravity. Thus in order to include the whole fibroglandular tissue in the defined breast region, the horizontal line had to be moved down posteriorly, which resulted in the inclusion of some portion of the body fat into the breast region. With the subject in prone position in breast MRI, the breast tissue was pulled away from the body, and vey little body fat was included in the breast region. However, two outliers were noted in the BV comparison, with BV acquired from LDCT remarkably lower than that acquired from MR. These two women had large breast (>1000 cm^3) but fatty breast tissue (PD=2.2% and 3.1% respectively). With a breast composition of small fibroglandular tissue volume, it was obvious that there was no need to move down the horizontal line. The BV measured from LDCT thus was smaller than that of MR. The FV acquired from LDCT also tended to be higher than the FV acquired from breast MRI. This might be due to different level of contrast between fat and fibroglandular tissues on LDCT and MRI, as well as the different segmentation algorithms that were used for the two modalities. LDCT simply used FCM but breast MRI used more sophisticated algorithm combining N3 and FCM. When using FCM in LDCT, a total cluster number of 9 or 10 was used, with 2 or 3 assigned for the fibroglandular tissue. This cluster setting was chosen based on visual inspection of the segmentation results on the relatively noisy LDCT images. For MRI, we have developed a very sophisticated iterative N3+FCM bias-field correction method that can also brighten the signal intensity of fatty tissues, and allow for an accurate segmentation between the two tissue types (18). Among the three outliers in FV comparison, all had dense fibroglandular tissue in MR (121.3, 188.0, and 316.7 cm^3, respectively).

This was a pilot study mainly reporting the development of a breast density quantification method based on LDCT images. Only a small number of Asian subjects were included in the

analysis. The obtained density results were further correlated with the density results from 3D MRI, which was used as the ground truth. It is obvious that the quality of LDCT was much inferior compared to the quality of MRI. Unlike 3D MRI, current density method for LDCT cannot be fully automatic yet. Operator intervention in some women, such as adjustment of the horizontal line to define the posterior boundary of the breast tissue, and the delineation and removal of pectoralis muscle, is still needed. However, with the technical improvement in LDCT and more robust segmentation algorithms, we believe the density segmentation results based on LDCT can be further improved in the future.

In conclusion, we have presented a quantitative breast density analysis method based on LDCT, and demonstrated that our segmentation method could yield a high reproducibility on the measured volume and percent breast density. The preliminary results found that the LDCT-measured density showed a high correlation with MR-measured density. The trend of larger BV measured by LDCT than MRI may be due to the different body positions in the two modalities. To further verify the role of LDCT-measured breast density for clinical practice, future large series studies are needed. As the use of LDCT for lung cancer screening increases, it may also provide valuable information about breast density for evaluating breast cancer risk.

Acknowledgement

This work was supported in part by NIH/NCI grant No. R01 CA127927, R21 CA170955, and R03 CA136071, and E-Da Hospital research grant No. EDAHP103007.

References

1. Boyd NF, Guo H, Martin LJ, et al. Mammographic density and the risk and detection of breast cancer. N Engl J Med. 2007; 356:227–236. [PubMed: 17229950]
2. Vachon CM, Brandt KR, Ghosh K, et al. Mammographic breast density as a general marker of breast cancer risk. Cancer Epidemiol Biomarkers Prev. 2007; 16:43–49. [PubMed: 17220330]
3. Boyd NF, Dite GS, Stone J, et al. Heritability of mammographic density, a risk factor for breast cancer. N Engl J Med. 2002; 347:886–894. [PubMed: 12239257]
4. Khazen M, Warren R, Boggis C, et al. Collaborators in the United Kingdom Medical Research Council Magnetic Resonance Imaging in Breast Screening (MARIBS) Study. A pilot study of compositional analysis of the breast and estimation of breast mammographic density using three-dimensional T1-weighted magnetic resonance imaging. Cancer Epidemiol Biomarkers Prev. 2008; 17:2268–2274. [PubMed: 18768492]
5. Nie K, Chen JH, Chan S, et al. Development of a quantitative method for analysis of breast density based on 3-dimensional breast MRI. Medical Physics. 2008; 35:5253–5262. [PubMed: 19175084]
6. Klifa C, Carballido-Gamio J, Wilmes L, et al. Magnetic resonance imaging for secondary assessment of breast density in a high-risk cohort. Magn Reson Imaging. 2010; 28:8–15. [PubMed: 19631485]
7. Saslow D, Boetes C, Burke W, et al. American Cancer Society Breast Cancer Advisory Group. American Cancer Society guidelines for breast screening with MRI as an adjunct to mammography. CA Cancer J Clin. 2007; 57:75–89. [PubMed: 17392385]
8. Menezes RJ, Roberts HC, Paul NS, et al. Lung cancer screening using low-dose computed tomography in at-risk individuals: the Toronto experience. Lung Cancer. 2010; 67:177–183. [PubMed: 19427055]
9. National Lung Screening Trial Research Team. Aberle DR, Adams AM, Berg CD, et al. Reduced lung- cancer mortality with low-dose computed tomographic screening. N Engl J Med. 2011; 365:395–409. [PubMed: 21714641]

10. Horeweg N, van Rosmalen J, Heuvelmans MA, et al. Lung cancer probability in patients with CT-detected pulmonary nodules: a prespecified analysis of data from the NELSON trial of low-dose CT screening. Lancet Oncol. 2014; 15:1332–1341. [PubMed: 25282285]
11. Chiumello D, Langer T, Vecchi V, et al. Low-dose chest computed tomography for quantitative and visual anatomical analysis in patients with acute respiratory distress syndrome. Intensive Care Med. 2014; 40:691–699. [PubMed: 24647812]
12. Carrillo MC, Alturkistany S, Roberts H, et al. Low-dose computed tomography (LDCT) in workers previously exposed to asbestos: detection of parenchymal lung disease. J Comput Assist Tomogr. 2013; 37:626–630. [PubMed: 23863542]
13. Larke FJ, Kruger RL, Cagnon CH, et al. Estimated radiation dose associated with low-dose chest CT of average-size participants in the National Lung Screening Trial. AJR Am J Roentgenol. 2011; 197:1165–1169. [PubMed: 22021510]
14. Padgett J, Biancardi AM, Henschke CI, Yankelevitz D, Reeves AP. Local noise estimation in low-dose chest CT images. Int J Comput Assist Radiol Surg. 2014; 9:221–229. [PubMed: 23877281]
15. Chen Y, Yang Z, Hu Y, et al. Thoracic low-dose CT image processing using an artifact suppressed large- scale nonlocal means. Phys Med Biol. 2012; 57:2667–2688. [PubMed: 22504130]
16. Moon WK, Lo CM, Goo JM, et al. Quantitative analysis for breast density estimation in low dose chest CT scans. J Med Syst. 2014; 38:21. [PubMed: 24643751]
17. Lin M, Chen JH, Wang X, Chan S, Chen S, Su MY. Template-based automatic breast segmentation on MRI by excluding the chest region. Med Phys. 2013; 40:122301. [PubMed: 24320532]
18. Lin M, Chan S, Chen JH, et al. A new bias field correction method combining N3 and FCM for improved segmentation of breast density on MRI. Med Phys. 2011; 38:5–14. [PubMed: 21361169]
19. Breast density and mammography reporting act of 2011. U.S. Congress; H.R. 1302 http://www.govtrack.us/congress/bill. Published October 2011. [November 15, 2011]
20. Ng KH, Yip CH, Taib NA. Standardization of clinical breast-density measurement. Lancet Oncol. 2012; 13:334–336. [PubMed: 22469115]
21. Laidevant AD, Malkov S, Flowers CI, Kerlikowske K, Shepherd JA. Compositional breast imaging using a dual-energy mammography protocol. Med Phys. 2010; 37:164–174. [PubMed: 20175478]
22. Maskarinec G, Morimoto Y, Daida Y, et al. Comparison of breast density measured by dual energy X- ray absorptiometry with mammographic density among adult women in Hawaii. Cancer Epidemiol Biomarkers Prev. 2011; 35:188–193.
23. Blackmore KM, Dick S, Knight J, Lilge L. Estimation of mammographic density on an interval scale by transillumination breast spectroscopy. J Biomed Opt. 2008; 13:064030. [PubMed: 19123676]
24. Blackmore KM, Knight JA, Lilge L. Association between transillumination breast spectroscopy and quantitative mammographic features of the breast. Cancer Epidemiol Biomarkers Prev. 2008; 17:1043–1050. [PubMed: 18483324]
25. Glide-Hurst CK, Duric N, Littrup P. Volumetric breast density evaluation from ultrasound tomography images. Med Phys. 2008; 35:3988–3997. [PubMed: 18841850]
26. Chen JH, Huang CS, Chien KC, et al. Breast density analysis for whole breast ultrasound images. Med Phys. 2009; 36:4933–4943. [PubMed: 19994502]
27. Salvatore M, Margolies L, Kale M, et al. Breast density: comparison of chest CT with mammography. Radiology. 2014; 270:67–73. [PubMed: 24126363]
28. Wang, XY.; Chen, JH.; Liao, YH.; Fwu, PT.; Lin, M.; Su, MY. Comparative measurement of breast volume and dense tissue volume based on breast MRI and low dose chest CT.. Presented at the 21th ISMRM Meeting (2013); Salt Lake City. May 20-26; p. 3366Program Number
30. Han T, Lai CJ, Chen L, Liu X, et al. Breast density measurement: 3D cone beam computed tomography (CBCT) images versus 2D digital mammograms. Proc of SPIE. 2009; 7258:72580L–1.
31. Huang SY, Boone JM, Yang K, et al. The characterization of breast anatomical metrics using dedicated breast CT. Med Phys. 2011; 38:2180–2191. [PubMed: 21626952]
32. Vedantham S, Shi L, Karellas A, O'Connell AM. Dedicated breast CT: Fibroglandular volume measurements in a diagnostic population. Med Phys. 2012; 39:7317–7328. [PubMed: 23231281]

33. Shih CT, Chang SJ, Liu YL, Wu J. Noise reduction of low-dose computed tomography using the multiresolution total variation minimization algorithm. Proc of SPIE. 2013; 8668:86682H–1.

34. Yu L, Manduca A, Jacobsen M, et al. Adaptive modulation of bilateral filtering based on a practical noise model for streaking and noise reduction in multi-slice CT. Proc. SPIE. 2010; 7622:762220.

35. Lindenbaum M, Fischer M, Bruckstein AM. On Gabor's contribution to image-enhancement. Pattern Recognition. 1994; 27:1–8.

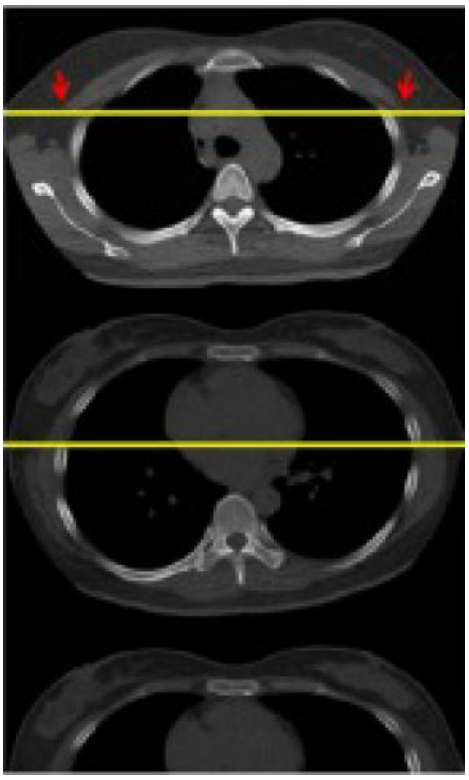

Figure 1.
Defining the posterior boundary of the breast at LDCT images. A horizontal line was drawn through the lateral margin of the bilateral pectoralis muscles (arrows) at the aortic arch level (upper). With this line, the operator checked all the slices and made sure the fibroglandular tissue was well-preserved (middle). A representative segmented breast image was generated (lower).

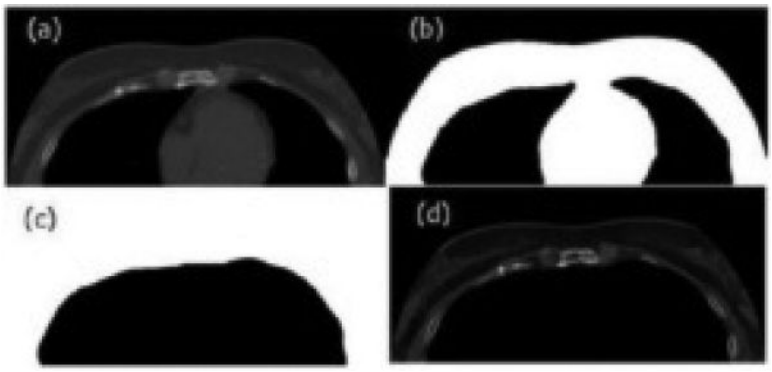

Figure 2.

Removal of the thoracic cavity region. (a) Original chest CT image. (b) The mask of the whole chest. (c) The mask of the thoracic cavity region (d) The image after removing the thoracic cavity region.

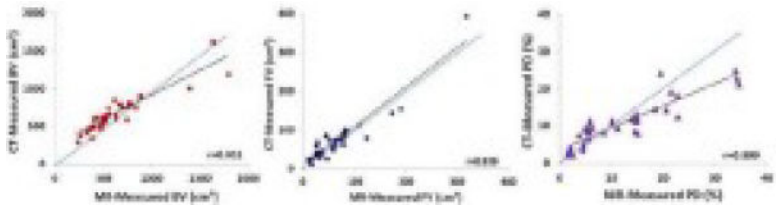

Figure 3.
Correlation of BV, FV, and PD measured from two imaging modalities.

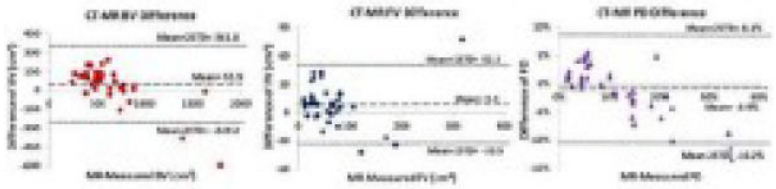

Figure 4.

Bland-Altman plots showing the absolute difference of measurement for BV, FV, and PD between two modalities, using MRI-measured results as the gold standard reference.

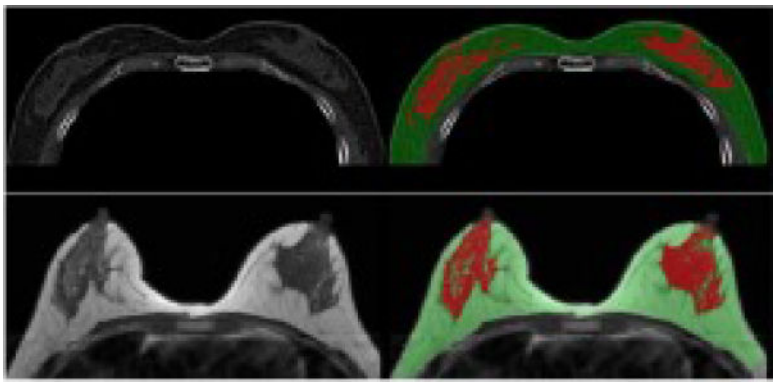

Figure 5.
Measurement of breast density with LDCT and MRI in a 45 y/o woman.

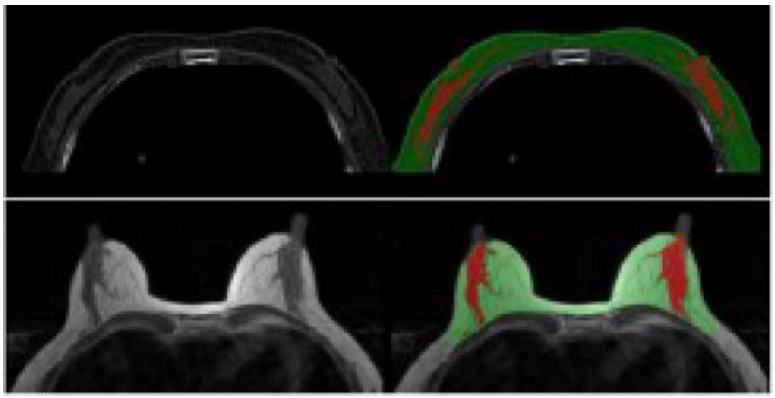

Figure 6.
Measurement of breast density with LDCT and MRI in a 55 y/o woman.

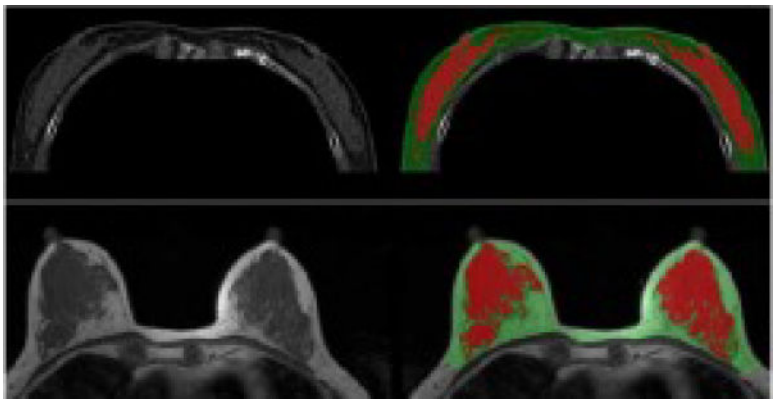

Figure 7.
Measurement of breast density with LDCT and MRI in a 62 y/o woman.

Table 1

Breast density values measured from MR and LDCT

	Breast Volume (cm^3)			Fiborglandular Tissue Volume (cm^3)			Percent Breast Density (%)		
	maxima	**minimum**	**mean±std**	**maxima**	**minimum**	**mean±std**	**maxima**	**minimum**	**mean±std**
MR (N=40)	1786.7	223.8	616.9±334.8	316.7	9.7	59.7±57.7	34.6	1.6	11.3 ±9.3
LDCT (N=40)	1620.5	296.4	672.8±239.9	394.4	13.0	69.0±62.3	25.2	2.2	10.4 ±6.1

Table 2

Results of breast density measurements in three women

		BV (Lt/Rt) (cm^3)	FV (Lt/Rt) (cm^3)	PD (Lt/Rt) (%)
Case-1 (Fig-5)	**LDCT**	646.3 / 654.5	70.4 / 76.3	10.9 / 11.7
	MRI	611.4 / 647.0	61.1 / 65.9	10.0 / 10.2
Case-2 (Fig-6)	**LDCT**	479.9 / 442.9	38.9 / 38.6	8.1 / 8.7
	MRI	350.7 / 331.4	30.4 / 27.9	8.7 / 8.4
Case-3 (Fig-7)	**LDCT**	517.2 / 510.5	101.4 / 97.9	19.6 / 19.2
	MRI	377.3 / 373.0	88.3 / 72.6	23.4 / 19.5

Lt: left breast; Rt: right breast